The role of diffusion in broadband infrared absorption in chalcogen-doped silicon

Brian R. Tull,[1] Mark T. Winkler,[2] and Eric Mazur[1,2,*]

[1]*School of Engineering and Applied Sciences, Harvard University, Cambridge, Massachusetts 02138*

[2]*Department of Physics, Harvard University, Cambridge, Massachusetts 02138*

(Dated: March 5, 2009)

Abstract

Sulfur doping of silicon beyond the solubility limit by femtosecond laser irradiation leads to near-unity broadband absorption of visible and infrared light and the realization of silicon-based infrared photodetectors. The nature of the infrared absorption is not yet well understood. Here we present a study on the reduction of infrared absorptance after various anneals of different temperatures and durations for three chalcogens (sulfur, selenium, and tellurium) dissolved into silicon by femtosecond laser irradiation. For sulfur doping, we irradiate silicon in SF_6 gas; for selenium and tellurium, we evaporate a film onto the silicon and irradiate in N_2 gas; lastly, as a control, we irradiated untreated silicon in N_2 gas. Our analysis shows that the deactivation of infrared absorption after thermal annealing is likely caused by dopant diffusion. We observe that a characteristic diffusion length—common to all three dopants—leads to the reduction of infrared absorption. Using diffusion theory, we suggest a model in which grain size of the re-solidified surface layer can account for this characteristic diffusion length, indicating that deactivation of infrared absorptance may be caused by precipitation of the dopant at the grain boundaries.

PACS numbers: 71.55.Cn, 78.30.Am, 61.72.uf

1. INTRODUCTION

Silicon is often doped with chalcogens to obtain optoelectronic properties not typically available to silicon-based devices, such as detection of infrared light,[1–4] and light emission (photoluminescence[5–8] and, more recently, electroluminescence[9,10]). In addition, the presence of the chalcogen atom in the silicon lattice is studied for its potential as a double donor.[11,12]

Doping is typically done by vapor diffusion during furnace annealing[5,8,12–14] or ion implantation followed by furnace annealing.[2,8,15–18] These methods have been used to establish the bulk diffusivity and equilibrium solubility limit of sulfur,[17,19,20] selenium,[21–25] and tellurium[14,18,23] in crystalline silicon.

When doping is performed via thermal diffusion, the concentration is restricted to the solubility limit at the annealing temperature; however, when ion implantation is followed by nanosecond pulsed laser irradiation,[26–29] the dopant concentration can exceed the solubility limit by several orders of magnitude through a process known as solute trapping.[30–32] This method has recently been used to create supersaturated concentrations of sulfur in silicon.[28] Recently, we created in silicon supersaturated concentrations of sulfur, selenium and tellurium, respectively, by femtosecond laser irradiation of silicon coated with a powder film.[33] We also doped silicon in this manner using a background gas of sulfur hexaflouride (SF_6) or hydrogen sulfide (H_2S).[34,35] In these recent studies involving nanosecond and femtosecond laser pulses, the supersaturated solution of chalcogen dopants exhibits increased infrared absorptance.[28,33–35] When femtosecond laser pulses are used, the infrared absorptance is near unity out to wavelengths of 2500 nm.[33–35]

The mechanism by which chalcogen-doped silicon absorbs infrared light is not entirely understood. Two observations provide insight into how the structural arrangement of the dopant contributes to the enhanced infrared absorption. First, the infrared absorption decreases after thermal annealing, and this decrease becomes larger with increasing annealing temperature.[28,33–35] Second, for the same anneal conditions, the decrease in infrared absorption depends on the dopant.[33] Sulfur-doped samples show the largest decrease in infrared absorption, followed by selenium-doped samples and tellurium-doped samples, respectively.[33] Given that the bulk diffusivity of sulfur in silicon is roughly an order of magnitude larger than selenium and several orders of magnitude larger than tellurium, the two experimental

observations indicate that the reduction of infrared absorptance after annealing is related to diffusion of the dopant.[33]

In this paper, we explore whether the deactivation of infrared absorption is a diffusion process by determining the optical properties of supersaturated chalcogen-doped silicon before and after thermal vacuum anneals. The silicon is doped by irradiation with femtosecond laser pulses in the presence of a background gas (for sulfur doping) or coated with an evaporated film of the dopant (for selenium and tellurium doping). Our analysis shows that thermal annealing reduces the infrared absorptance in a manner that is consistent with diffusion of the dopant. In addition, the drop in infrared absorptance is associated with a characteristic diffusion length that is on the same lengthscale for all three dopants (S, Se, Te). Using diffusion theory, we show that a probable source of this characteristic diffusion length is the grain size of the re-solidified surface layer.

2. EXPERIMENTAL SETUP

For all experiments, we used boron-doped Si (100) wafers ($\rho = 1 - 20$ Ω·cm), ultrasonically cleaned in methanol for 10 minutes. For sulfur doping, the wafers were placed on a translation stage in a stainless steel vacuum chamber that was evacuated to less than 2 Pa using a mechanical pump. The chamber was filled with SF_6 at a pressure of 6.7×10^4 Pa. For selenium and tellurium doping, the wafers were first placed into a resistive thermal evaporator that was evacuated to 2×10^{-4} Pa. A film thickness of 150 nm was deposited for both selenium and tellurium using solid selenium (99.95%) and tellurium (99.95%) pellets, respectively, in tungsten boat sources. The coated wafers were loaded into the stainless steel vacuum chamber, which was then evacuated to less than 2 Pa and filled with 6.7×10^4 Pa of N_2. Femtosecond laser ablation in a gas of near-atmospheric pressure results in different hydrodynamics for melting and ablation than irradiation performed in a vacuum.[36] In order to keep the hydrodynamics of doping the same for all samples, we irradiated the selenium- and tellurium-coated samples in a background gas of N_2 at the same pressure as the samples irradiated in SF_6.

We irradiated the wafers with a 1-kHz train of 100-fs, 800-nm laser pulses with a fluence of 8 kJ/m^2 focused to a full-width at half-maximum spot size of 150μm. The wafer's surface was perpendicular to the incident laser and translated in the plane of the surface with a

speed of 1.5 mm/s; thus we expose every point on the surface to 100 laser pulses. A 33 mm x 33 mm area was irradiated on each wafer by translating 33 mm vertically, stepping 75 μm horizontally and repeating.

After irradiation, the wafers were removed and cut into 8 mm x 11 mm samples for annealing in a thermal vacuum oven evacuated to less than 2×10^{-4} Pa. We evaluated the optical properties of the samples before and after annealing by measuring the infrared absorptance with a UV-VIS-NIR spectrophotometer equipped with an integrating sphere detector. The diffuse and specular reflectance (R) and transmittance (T) were measured for the wavelength range of 0.9–2.5 μm, in 1-nm increments to determine the absorptance ($A = 1 - R - T$) at each wavelength.

We performed twenty-five thermal vacuum anneals covering a matrix of five temperatures (575 K, 675 K, 775 K, 875 K, 975 K) and five durations (10 min, 30 min, 100 min, 6 h, 24 h) for each of the four types of samples: Si wafers irradiated in SF_6; Si wafers coated with selenium or tellurium and irradiated in N_2; and Si wafers irradiated in N_2. To explore the high temperature behavior, the four types of samples were annealed to temperatures between 975 K and 1175 K for 100 min. Lastly, as a control, an untreated Si wafer was annealed to 1175 K for 100 min.

3. RESULTS

After irradiation, the surface of each sample is transformed from a flat, mirror-finished, light gray wafer into a visibly matte black or dark gray surface. Inspection with a scanning electron microscope reveals that the surface is covered with a forest of micrometer-sized spikes. The formation of this surface morphology is a function of the laser wavelength, fluence, and pulse duration, as well as the gas chemistry and pressure; the mechanism behind its formation has been well documented elsewhere.[37,38]

Figure 1 compares the infrared absorptance of each of the four types of samples after laser irradiation to the absorptance of the initial silicon wafer. The initial silicon wafer is largely transparent to wavelengths of light greater than 1.1 μm due to the band gap energy of crystalline silicon. The chalcogen-doped samples exhibit near unity absorptance of infrared light and samples irradiated in N_2 show some infrared absorptance, which decreases with increasing wavelength.

Figure 2 shows the infrared absorptance of the chalcogen-doped samples after annealing at 775 K for the five different time durations. The infrared absorptance of all three samples is reduced after annealing; this reduction increases with annealing time. Sulfur-doped samples show the largest decrease in infrared absorptance, followed by selenium-doped samples; the absorptance of tellurium-doped samples changes the least.

Figure 3 displays the mean infrared absorptance between 1.2 μm and 2.5 μm after annealing for each of the four types of samples: sulfur-doped (circles) selenium-doped (squares), tellurium-doped (triangles) and samples irradiated in N_2 (diamonds). The size of the marker indicates the length of each anneal, with the largest size equaling 24 h and the smallest, 10 min. Additionally, data for an unprocessed silicon wafer annealed at 1175 K is shown (black dot). Between 575 K and 875 K, the change in absorptance has the same trend for all three chalcogen-doped samples; absorptance drops with increasing anneal temperature and at a given temperature, a longer annealing time results in a further decrease in absorptance. At 875 K, the absorptance of the sulfur-doped samples and the samples irradiated in N_2 have been reduced to the infrared absorptance of the original unirradiated silicon substrate. Above 875 K, the change in absorptance of each sample has a different trend. The absorptance of sulfur-doped samples and those irradiated in N_2 begins to increase with increasing temperature. The absorptance of selenium-doped samples stays at approximately the same value as at 875 K and the absorptance of tellurium-doped samples continues to decrease.

4. DISCUSSION

Crystalline silicon is mostly transparent to light wavelengths longer than 1.1 μm due to its band gap. The absorptance of light wavelengths shorter than 1.1 μm depends on the roughness of the silicon surface. All samples that we irradiate in this study exhibit enhanced absorption of light wavelengths shorter than 1.1 μm (see Figure 1)[34,35,37,39]. This observation is also true for samples irradiated in vacuum[37]; the enhanced absorption in this wavelength region is caused by multiple reflections on the textured surface.

If irradiation is performed in the presence of certain dopants, such as sulfur, selenium or tellurium, the absorptance of infrared light between 1.1–2.5 μm is enhanced to near-unity (see Figure 1). However, this behavior is not observed for all dopants, such as the samples irradiated in N_2 gas (see Figure 1). The N_2 samples exhibit a non-uniform absorptance

of infrared light, which decreases with increasing wavelength. This same behavior is seen when silicon is irradiated in many other gases[34,35,37,39] (H_2, Cl_2, and air) as well as when irradiation is performed in a vacuum.[37] Because the optical behavior of silicon irradiated in the presence of non-chalcogens is similar to vacuum, we attribute this infrared absorptance to structural defects present in the nanocrystalline grains and not to doping of the silicon with species in the background gas.

In order to understand the mechanism of the near-unity infrared absorptance between 1.1 and 2.5 μm, we begin by reviewing what is known about the structure and composition of femtosecond laser-doped silicon. During irradiation of silicon with ultrashort laser pulses above the ablation threshold[40] (3 kJ/m^2) the top surface layer is ablated away and the next layer below the surface melts. This thin molten layer resolidifies extremely quickly due to its contact with the cold bulk substrate. Cooling rates are estimated to be as high as 10^{15} K/s.[41] When a gas or surface dopant is present during irradiation it is atomized by the high intensity of the ultrashort laser pulse and mixes with the molten silicon. Rutherford back scattering measurements[33–35] show that these gas or surface dopant species are incorporated at a concentration on the order of 1 atomic percent and that 20–70% of the dopants are located on substitutional lattice sites.[35] This concentration is orders of magnitude above the equilibrium solubility limit and the dopants are therefore in a supersaturated solution.[33] The high concentration of dissolved atoms become trapped in the lattice during the extremely fast resolidification in a process that is similar to the solute trapping that occurs after pulsed laser irradiation of ion implanted semiconductors.[29] Cross-sectional transmission electron microscopy reveals that the resolidified surface layer is an approximately 300-nm thick polycrystalline layer with nanometer-sized grains (10–50 nm).[35] It is this surface layer that contains the supersaturated concentration of dopants and is responsible for the resulting optical properties.

We previously proposed that the broadband absorptance of infrared light is caused by the high concentration of chalcogen dopants in the nanometer sized grains of the polycrystalline surface layer.[33–35] An equilibrium concentration of sulfur, selenium or tellurium atoms creates deep level donors in the band gap of silicon.[12,13] A supersaturated concentration of chalcogen atoms creates a densely populated impurity band around one or more of those deep levels. Below, we provide support for this mechanism by suggesting a simple diffusion model that demonstrates that, upon annealing, the decrease in absorptance scales with the fraction of

dissolved dopants that diffuse out of the nanometer-sized grains to the grain boundaries. Diffusion of the dopants out of the grains reduces the number of impurity levels in the band gap and thus reduces the infrared absorption. Because the grains are on the order of nanometers in size, thermal anneals that cause diffusion on the order of nanometers decrease the absorptance.

Precipitation of the dopant within the crystalline grains via clustering of dopant atoms could also lead to deactivation of infrared absorption. With the analysis described below, it is difficult to distinguish whether clustering or diffusion to the grain boundaries is responsible for the observed drop in infrared absorptance because both processes involve diffusion of the dopant on a length scale on the order of nanometers through the crystalline grains. The current work identifies diffusion as the relevant process regardless of whether clustering or relocation to a grain boundary is the appropriate boundary condition.

For every thermal anneal, we can estimate the diffusion length $d = \sqrt{Dt}$ for each dopant (sulfur, selenium and tellurium), where t is the annealing time; D is the bulk diffusivity for each dopant in silicon given by $D = D_0 \exp(-E_a/(kT))$; T is the annealing temperature; k is the Boltzmann constant; and D_0 and E_a are temperature-independent constants obtained from the literature on the bulk diffusivity of sulfur, selenium and tellurium in silicon. For each anneal, the temperature and annealing time is known; the diffusivity of the dopant can be calculated using the temperature and a diffusion length can be obtained for each anneal for sulfur, selenium and tellurium, respectively. It is important to note that, when considering diffusion length, our annealing data set contains redundant data points: for example, a long low-temperature anneal yields the same diffusion length as a short higher temperature anneal. If the decrease in infrared absorptance is a diffusion-related phenomenon, we should observe similar results from time-temperature data points that correspond to the same diffusion length; we will see that this is indeed the case.

Slightly different values for D_0 and E_a for each dopant have been reported in the literature.[14,17–25] For our analysis, we chose diffusivity constants determined from studies that used the lowest temperature range and a similar silicon substrate (see Table I). For tellurium, the referenced study fit its data as the sum of two Arrhenius curves, giving high temperature and low temperature values for D_0 and E_a; in that case we used the low temperature values. Although our analysis is carried out with one set of diffusion constants for each dopant, all reported diffusivities yield similar results and lead to the same conclusions.

In Figure 4, we again plot the infrared absorptance from Figures 3; however, now the data for sulfur-doped (circles), selenium-doped (squares) and tellurium-doped (triangles) samples are plotted versus the diffusion lengths of sulfur, selenium and tellurium atoms, respectively (these diffusion lengths are calculated using the constants in Table I). In addition, the infrared absorptance is normalized so that the maximum value is the preannealed infrared absorptance from Figure 1 and the minimum value is the infrared absorptance of the unirradiated silicon wafer.

We can draw several conclusions from Figure 4. First, the infrared absorptance decreases monotonically with diffusion length with some exceptions at large diffusion length, which we address below. Second, the infrared curve for each chalcogen-doped sample decreases at diffusion lengths that are of the same order of magnitude as the observed grain size of femtosecond laser irradiated silicon ($10-50$ nm).[35] Third, all anneals that yield a particular diffusion length, but are performed with varying time-temperature combinations, result in roughly the same decrease in infrared absorptance. For example, 24 h at 575 K yields roughly the same diffusion length and decrease in infrared absorptance as 10 min at 675 K, for all three dopants (similarly for 24 h at 675 K and 10 min at 775 K, or 24 h at 775 K and 10 min at 875 K). Finally, when the data is normalized to the diffusion length of each sample dopant, the infrared absorptance decreases at the same rate for all three samples; in other words, the data suggests a characteristic diffusion length associated with the deactivation of infrared absorptance. These observations are strong evidence that the reduction of absorptance is a diffusion related process.

We believe the increase of infrared absorptance in some samples at high temperature anneals is caused by impurities introduced during the high temperature process. The evidence for this conclusion is the manifestation of this infrared absorptance in the unprocessed silicon wafer (black dot in Figure 3). The high temperature data points showing increased infrared absorption at high temperatures are, for the rest of our analysis, considered anomalous and not presented. Even if the increase were a more meaningful phenomenon, it falls outside the bounds of our current analysis and model, and is presented only for completeness.

4.1. Diffusion theory

If the decrease in infrared absorptance is caused by the diffusion of dopants out of the crystalline grains, we can use diffusion theory to estimate how the concentration of dopant atoms in the grains should decrease with thermal annealing, and compare this decrease to our data. We begin by making the following simplifying assumptions: the crystalline grains are spherical with a fixed radius R_0 and an initial dopant concentration C_0 spreads uniformly throughout the grains; diffusion occurs radially out from the center; the grain boundaries are perfect sinks (*i.e.*, once a dopant atom reaches the grain boundary, it does not diffuse back into the grain); the diffusivity of the dopant is only a function of temperature and does not vary with concentration.

In order to treat the grain boundaries as a perfect sink for the dopant, we set the boundary condition $C(R_0) = C_e$ for all t, where C_e is the equilibrium dopant concentration at the annealing temperature (which is several orders of magnitude below the initial dopant concentration); the dopant concentration in the grain does not drop below this value during the anneal. We make an additional assumption that the equilibrium dopant concentration is not sufficient to bring about enhanced broadband infrared absorption, which is consistent with research on silicon doped with chalcogens at or below the equilibrium concentration.[13] Because the concentration in the grain cannot decrease below C_e, we treat this value as a background concentration and express our concentration profile as $\tilde{C}(r,d) = C(r,d) - C_e$.

With these assumptions the concentration profile, $\tilde{C}(r)$, in the grain is given by

$$\tilde{C}(r,d) = -\frac{2R_0\tilde{C}_0}{\pi r}\sum_{n=1}^{\infty}\frac{(-1)^n}{n}\sin\left(\frac{n\pi r}{R_0}\right)\exp\left[-\left(\frac{n\pi d}{R_0}\right)^2\right], \tag{1}$$

where $\tilde{C}(r,d) = C(r,d) - C_e$ is the increased concentration above the equilibrium value at a distance r from the center of the sphere after a thermal anneal that produces a dopant diffusion length of $d = \sqrt{Dt}$; and $\tilde{C}_0 = C_0 - C_e$ is the initial increased concentration above the equilibrium value. Equation 1, divided by $\tilde{C}_0$, is equivalent to $1 - C(r,d)/C_0$ for a sphere that is absorbing solute from a large volume of well-stirred liquid with a fixed concentration of C_0.[42]

We can determine the number of dopant atoms, $\tilde{N} = N - N_e$, above the equilibrium value in the sphere after a thermal anneal with diffusion length, d, by integrating Eq. 1 over the volume of the sphere (radius R_0). If we then divide by the initial number of dopant atoms in

the sphere that exceeds the equilibrium value, $\tilde{N}_0 = \frac{4}{3}\pi R_0^3 \tilde{C}_0$, to obtain the fraction, $\tilde{N}/\tilde{N}_0$, of supersaturated dopant atoms remaining in the sphere after annealing (a dimensionless number between 0 and 1), we obtain:

$$\frac{\tilde{N}(d)}{\tilde{N}_0} = \frac{\int_0^{R_0} \tilde{C}(r,d) 4\pi r^2 dr}{\frac{4}{3}\pi R_0^3 \tilde{C}_0} = \frac{6}{\pi^2} \sum_{n=1}^{\infty} \frac{1}{n^2} \exp\left[-\left(\frac{n\pi d}{R_0} \right)^2 \right]. \tag{2}$$

The resulting fraction is only a function of diffusion length, d, and the radius of the sphere, R_0. The grain sizes are likely to follow a lognormal distribution:[42]

$$y(R_0) = A \exp\left(-\left(\frac{\ln(R_0/p)}{w} \right)^2 \right), \tag{3}$$

where y is the number of grains with radius, R_0; p is the peak radius with height, A, and width, w. To account for this lognormal distribution of grain sizes, we perform a summation of curves calculated from Eq. 2 for grain sizes ranging from $R_0 = 1$ to 5000 nm at 1 nm increments. The summation is weighted by volume,

$$\left(\frac{\tilde{N}(d)}{\tilde{N}_0} \right)_{lognormal} = \frac{\sum_{R_0=1}^{5000} \left(\frac{\tilde{N}(d)}{\tilde{N}_0} \right)_{R_0} y(R_0)(\frac{4}{3}\pi R_0^3)}{\sum_{R_0=1}^{5000} y(R_0)(\frac{4}{3}\pi R_0^3)}. \tag{4}$$

where $y(R_0)$ is the number of grains with radius, R_0, and $\left(\frac{\tilde{N}(d)}{\tilde{N}_0} \right)_{R_0}$ is the fraction of supersaturated dopants remaining in a sphere of radius, R_0, as a function of diffusion length. The sum, $\sum_{R_0=1}^{5000} y(R_0)(\frac{4}{3}\pi R_0^3)$, is the total volume of all the grains in the lognormal distribution.

Equation 4 is plotted in Figure 5 for a monodisperse distribution of 5-nm radius grains and four lognormal distributions with $A = 150$, $p = 5$ nm and $w = 0.5$, 0.75, 1 and 1.25. As the width, w, of the lognormal distribution increases, the slope of the curve becomes smaller, more closely matching the slope of the data. This result is reasonable as larger grains lose dopants more slowly than smaller grains; therefore, adding larger grains to the distribution decreases the slope of the fraction of supersaturated dopants remaining in the grains.

4.2. Comparison to diffusion theory

The six curves in Figure 4 were obtained from Eq. 2 using radii that are similar to the grain sizes observed in femtosecond laser irradiated silicon.[35] In spite of the simplicity of

our theoretical model, the qualitative agreement is remarkably good. The general shape and order of magnitude of these data agree well with our model for all three dopants. Our model does not take into account the possibility of grain growth, changes in diffusivity with concentration, or a change in activation energy when diffusing from the grain to the grain boundary. Below we discuss the deviations between the data and our theoretical model and speculate on possible explanations.

At large diffusion lengths (> 100 nm), the infrared absorptance of sulfur-doped samples begins to increase. This increase is also exhibited by samples irradiated in N_2 and untreated silicon wafers after annealing. The cause of this increase is not known, but it is related to the original substrate and not the presence of the sulfur dopants. The samples annealed at high temperatures could have absorbed contamination from the vacuum furnace, altering their infrared absorptance. This contamination is likely to contribute to the deviation of selenium- and tellurium-doped samples from the theory by slowing their decrease in absorptance.

At small diffusion lengths, the absorptance data does not decrease as fast as theory predicts, and the deviation increases as diffusion length increases. One potential reason for this behavior is buildup of dopants at the grain boundaries. As more dopants diffuse from the crystalline grains to the grain boundaries, less surface is available, causing diffusion from the grains to be increasingly more difficult. We can estimate the number of dopants that can fit in the free space available at the grain boundary as,

$$N_{GB} = \frac{1}{2}\rho_i a(4\pi R_0^2), \tag{5}$$

where ρ_i is the atomic density of the dopant (on the order of 3–4 $\times 10^{22}$ cm^{-3} for sulfur, selenium, and tellurium), a is the width of the grain boundary (on the order of the lattice parameter of silicon, 0.54 nm, and $4\pi R_0^2$ is the surface area of the grain. The factor 1/2 in Eq. 5 accounts for the fact that that each grain boundary is shared by two grains. We compare this value to the number of dopant atoms in the grain which can be expressed as,

$$N_G = \frac{4}{3}\pi R_0^3 C_i, \tag{6}$$

where C_i is the dopant concentration ($\sim 5 \times 10^{20}$ cm^{-3}) and $\frac{4}{3}\pi R_0^3$ is the volume of the grain. For a grain size of $R_0 = 10$ nm, N_G/N_{GB} is 0.16. This value increases as grain size increases. For a grain size of $R_0 = 60$ nm, N_G/N_{GB} already exceeds 1, indicating that buildup at the

grain boundaries could slow diffusion for grains of size $R_0 \geq 60$ nm for concentrations on the order of 1 atomic percent.

5. CONCLUSION

Our analysis shows that the decrease in near-unity broadband infrared absorptance of supersaturated chalcogen-doped silicon after thermal annealing is most likely caused by dopant diffusion. We observe that a characteristic diffusion length of about 50 nm common to all three dopants leads to the deactivation of infrared absorption. If we assume the diffusivity of each dopant in our samples is similar to the bulk diffusivity reported in the literature, the grain size of the re-solidified surface layer probably sets this characteristic diffusion length, especially for a lognormal distribution of grain sizes. We propose that a probable cause of the deactivation of infrared absorption is precipitation of the dopant at the grain boundaries. It is possible that other mechanisms, such as precipitation of dopant particles within the grains in the form of clustering, also lead to the deactivation of infrared absorption. Further work on annealing studies of supersaturated chalcogen-doped silicon with different grain size distributions as well as in single crystalline silicon will help determine the relative contribution of each mechanism as a function of the silicon's microstructure and the dopant concentration.

Acknowledgments

Several people contributed to the work described in this paper. B.T. conceived the basic idea, designed the experiment, and collected and analyzed the data; M.W. provided assistance with the analysis. E.M. supervised the research and development of the manuscript. The authors are very grateful for helpful discussions with Mike Aziz. This work was supported by the Army Research Office under contact W911NF-05-1-0341. M.W. acknowledges the National Science Foundation Graduate Research Program for financial support.

* Electronic address: mazur@physics.harvard.edu

[1] H. R. Vydyanath, W. J. Helm, J. S. Lorenzo, and S. T. Hoelke, Infrared Physics **19**, 93 (1979).

[2] N. Sclar, Journal of Applied Physics **52**, 5207 (1981).

[3] J. E. Carey, C. H. Crouch, M. Shen, and E. Mazur, Optical Letters **30**, 1773 (2005).

[4] Y. A. Astrov, L. M. Portsel, A. N. Lodygin, V. B. Shuman, and E. V. Beregulin, in *Gettering and Defect Engineering in Semiconductor Technology XI* (2005), Solid State Phenomena 108-109, pp. 401–406.

[5] X. Zhang, M. Kleverman, and J. Olajos, Semiconductor Science and Technology **14**, 1076 (1999).

[6] A. Henry, J. Svensson, E. Janzen, and B. Monemar, Materials Science and Engineering B-Solid State Materials for Advanced Technology **4**, 261 (1989).

[7] T. G. Brown and D. G. Hall, Applied Physics Letters **49**, 245 (1986).

[8] T. G. Brown, P. L. Bradfield, and D. G. Hall, Applied Physics Letters **51**, 1585 (1987).

[9] M. A. Lourenco, M. Milosavljevic, S. Galata, M. S. A. Siddiqui, G. Shao, R. M. Gwilliam, and K. P. Homewood, Vacuum **78**, 551 (2005).

[10] J. Bao, M. Tabbal, T. Kim, S. Charnvanichborikarn, J. S. Williams, M. J. Aziz, and F. Capasso, Optics Express **15** (2007).

[11] M. Thiagarajan, K. Iyakutti, and E. Palaniyandi, Physica Status Solidi B-Basic Research **205**, 553 (1998).

[12] H. G. Grimmeiss, E. Janzen, H. Ennen, O. Schirmer, J. Schneider, R. Worner, C. Holm, E. Sirtl, and P. Wagner, Physical Review B **24**, 4571 (1981).

[13] E. Janzen, R. Stedman, G. Grossmann, and H. G. Grimmeiss, Physical Review B **29**, 1907 (1984).

[14] E. Janzen, H. G. Grimmeiss, A. Lodding, and C. Deline, Journal of Applied Physics **53**, 7367 (1982).

[15] R. G. Wilson, Journal of Applied Physics **55**, 3490 (1984).

[16] A. A. Taskin, B. A. Zaitsev, V. I. Obodnikov, and E. G. Tishkovskii, Semiconductors **34**, 312 (2000).

[17] F. Rollert, N. A. Stolwijk, and H. Mehrer, Applied Physics Letters **63**, 506 (1993).

[18] F. Rollert, N. A. Stolwijk, and H. Mehrer, Materials Science and Engineering B-Solid State Materials for Advanced Technology **18**, 107 (1993).

[19] P. L. Gruzin, S. V. Zemskii, A. D. Bulkin, and N. M. Makarov, Soviet Physics Semiconductors-Ussr **7**, 1241 (1974).

[20] R. O. Carlson, R. N. Hall, and E. M. Pell, Journal of Physics and Chemistry of Solids **8**, 81 (1959).

[21] N. S. Zhdanovich and Y. I. Kozlov, Soviet Physics Semiconductors-USSR **10**, 1102 (1976).

[22] H. R. Vydyanath, J. S. Lorenzo, and F. A. Kroger, Journal of Applied Physics **49**, 5928 (1978).

[23] H. Stumpel, M. Vorderwulbecke, and J. Mimkes, Applied Physics A-Materials Science and Processing **46**, 159 (1988).

[24] C. S. Kim and M. Sakata, Japanese Journal of Applied Physics **18**, 247 (1979).

[25] H. G. Grimmeiss, E. Janzen, B. Skarstam, and A. Lodding, Journal of Applied Physics **51**, 6238 (1980).

[26] C. W. White, S. R. Wilson, B. R. Appleton, and F. W. Young, Journal Of Applied Physics **51**, 738 (1980).

[27] E. M. Lawson, Journal of Applied Physics **53**, 6459 (1982).

[28] T. G. Kim, J. M. Warrender, and M. J. Aziz, Applied Physics Letters **88** (2006).

[29] S. U. Campisano, G. Foti, P. Baeri, M. G. Grimaldi, and E. Rimini, Applied Physics Letters **37**, 719 (1980).

[30] M. J. Aziz, Journal of Applied Physics **53**, 1158 (1982).

[31] M. J. Aziz, J. Y. Tsao, M. O. Thompson, P. S. Peercy, and C. W. White, Physical Review Letters **56**, 2489 (1986).

[32] J. A. Kittl, P. G. Sanders, M. J. Aziz, D. P. Brunco, and M. O. Thompson, Acta Materialia **48**, 4797 (2000).

[33] M. A. Sheehy, B. R. Tull, C. M. Friend, and E. Mazur, Materials Science and Engineering B-Solid State Materials for Advanced Technology **137**, 289 (2006).

[34] M. A. Sheehy, L. Winston, J. E. Carey, C. M. Friend, and E. Mazur, Chemistry of Materials **17**, 3582 (2005).

[35] C. H. Crouch, J. E. Carey, M. Shen, E. Mazur, and F. Y. Genin, Applied Physics A-Materials Science and Processing **79**, 1635 (2004).

[36] B. R. Tull, J. E. Carey, M. A. Sheehy, C. Friend, and E. Mazur, Applied Physics A-Materials

Science and Processing **83**, 341 (2006).

[37] J. E. Carey, Ph.D. thesis, Harvard University (2004).

[38] B. R. Tull, J. E. Carey, E. Mazur, J. McDonald, and S. M. Yalisove, Materials Research Society Bulletin **31**, 626 (2006).

[39] R. J. Younkin, J. E. Carey, E. Mazur, J. A. Levinson, and C. M. Friend, Journal of Applied Physics **93**, 2626 (2003).

[40] D. von der Linde and K. Sokolowski-Tinten, Applied Surface Science **154**, 1 (2000).

[41] T. E. Glover, Journal Of The Optical Society Of America B-Optical Physics **20**, 125 (2003).

[42] J. Crank, *The Mathematics of Diffusion* (Clarendon Press, Oxford, 1956), 1st ed.

TABLE I: Diffusivity constants

Dopant Element	$D_0(\mathrm{cm}^2/\mathrm{s})$	$E_a(\mathrm{eV})$
S (Ref. 20)	0.92	2.2
Se (Ref. 22)	2.47	2.84
Te (Ref. 18)	0.048	3.04

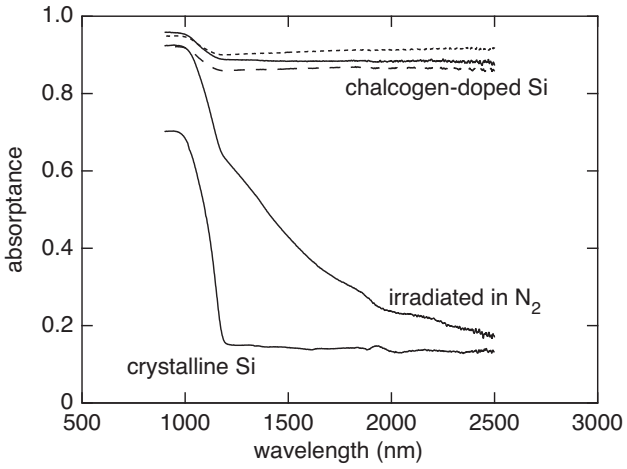

FIG. 1: Absorptance spectra for samples irradiated in the presence of sulfur hexafluoride (solid line), selenium (dashed line), tellurium (dotted line), and nitrogen gas (solid line) prior to thermal annealing. The absorptance of the untreated, crystalline silicon wafer is included for comparison.

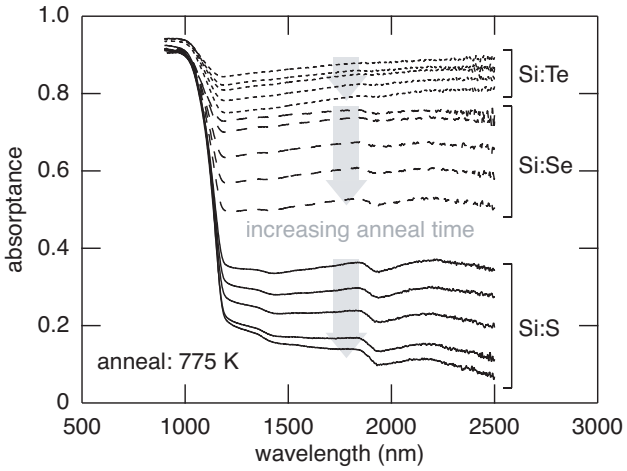

FIG. 2: Absorptance spectra for sulfur-, selenium-, and tellurium-doped silicon after annealing to 775 K for increasing lengths of time (from top to bottom: 10 min, 30 min, 100 min, 6 h, 24 h).

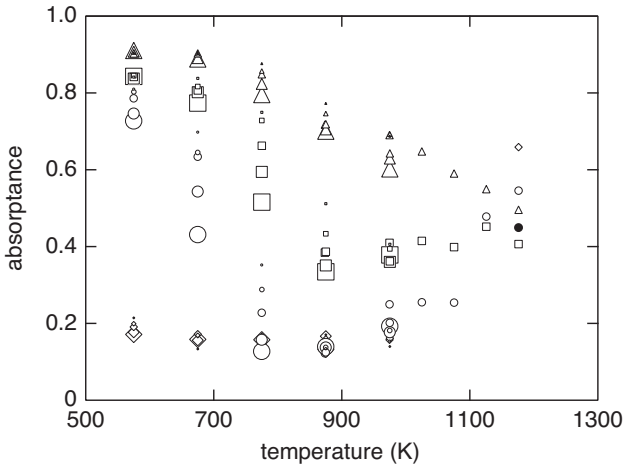

FIG. 3: Average absorptance from 1250–2500 nm for sulfur-doped (circles), selenium-doped (squares), tellurium-doped (triangles) silicon and samples irradiated in N_2 (diamonds) after various thermal anneals at $T \leq 975$ K. A larger marker indicates a longer anneal (from smallest to largest: 10 min, 30 min, 100 min, 6 h, 24 h).

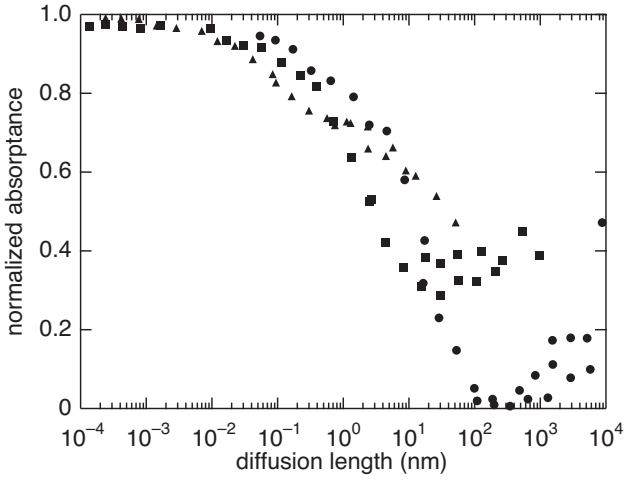

FIG. 4: Normalized absorptance for sulfur-doped (circles), selenium-doped (squares), and tellurium-doped (triangles) silicon after various thermal anneals versus diffusion length of the respective dopant. The average infrared absorptance from Figures 3 has been renormalized so that the maximum is the preannealed value and the minumum is the infrared absorptance of the unirradiated silicon wafer (see Figure 1).

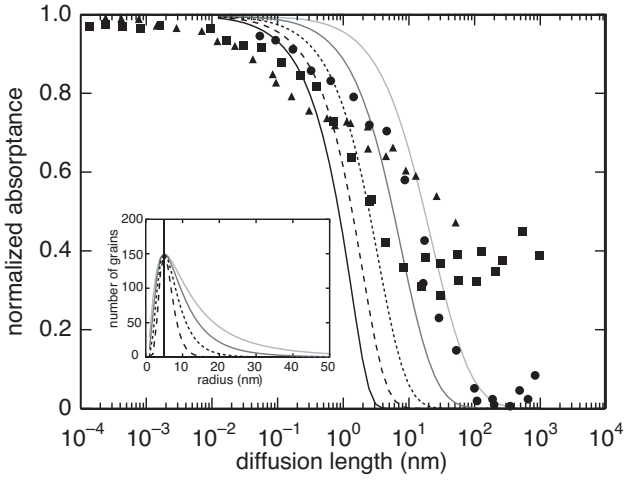

FIG. 5: Plot of Equation 4 for the five grain size distributions shown in the inset, overlaid on the data from Fig. 4 ($A = 150$, $p = 5$ nm, $y_0 = 0$ and $w = 0.5$, 0.75, 1 and 1.25). The solid black line represents a monodisperse distribution of grains with $R_0 = 5$ nm.